Microscopic optical potential for ^{4}He scattering based on the effective Skyrme interaction

V. I. Kuprikov and V. V. Pilipenko*

National Science Center "Kharkov Institute of Physics and Technology", 1 Akademichna Street, Kharkov 61108, Ukraine

(Received 29 July 2016; revised manuscript received 6 October 2016; published 20 December 2016)

Microscopic optical potential of ^{4}He interaction with nuclei is constructed by means of the single-folding model using the nucleon-nucleus optical potentials, which earlier were successfully applied to describing the neutron and proton scattering and are obtained from approximate calculations of the mass operator of the one-particle Green's function with the effective Skyrme nucleon-nucleon forces. The ^{4}He scattering processes are described in a self-consistent approach based on the standard and extended Skyrme forces, which simultaneously provide a satisfactory description of nuclear structure and nucleon-nucleus scattering. The performed calculations reasonably describe experimental data on differential cross sections of the elastic and inelastic α-particle scattering on different target nuclei in the mass-number range from ^{28}Si to ^{208}Pb at different projectile energies below or about 100 MeV, as well as the energy dependences of α-particle reaction cross sections on nuclei in a wide energy range.

DOI: 10.1103/PhysRevC.94.064612

I. INTRODUCTION

Elaboration of theoretical approaches that include both calculations of structures of atomic nuclei and descriptions of collision processes of nucleons or composite light nuclei (e.g., deuterons and α particles) with nuclei, based on certain realistic effective nucleon-nucleon interactions, is an important problem of modern nuclear physics. In this framework, among the most frequently employed models are those using microscopic optical potentials (MOP) along with nuclear structure description using the microscopic shell model. Different models of MOP for describing nuclear scattering processes have been developed, which are based on using various effective nucleon-nucleon (NN) forces and realistic nuclear densities.

In the literature, a frequently used approach to building nucleon-nucleus (NA) and nucleus-nucleus MOP is based on folding models (see, for example, Refs. [1–3]). When considering scattering processes with composite projectiles, in particular ^{4}He, the subject of the present article, many authors (see, for example, Refs. [2,4–6] and references therein) make use of the double-folding model (DFM), in which the optical potential is obtained by doubly folding an effective NN interaction with the nucleon density distributions of both the target nucleus and projectile. On the other hand, such processes are also described on the basis of approximation using the single-folding model (SFM) of the projectile density with the NA optical potential, which can also be constructed in a microscopic approach (see, for example, Refs. [6,7]). In these folding MOP models, as a rule (see Ref. [1–7]), the effective NN interaction is taken in the form resulting from the g-matrix consideration, e.g., Refs. [8–13]. Note that to describe experimental data satisfactorily, in most calculations by both DFM and SFM it is necessary to introduce adjustable renormalization parameters of the calculated MOP. However, there are examples of folding MOP calculations that do not make use of any renormalizations. For instance, in the work of Ref. [6] authors succeeded in describing α-particle–nucleus (αA) scattering cross sections with no fitting parameters in both DFM and SFM approaches on the basis of the Melbourne g-matrix effective NN interaction [3]. Also, in Ref. [6], it was shown that the results of calculations in the SFM approximation can agree well enough with those of the DFM calculations under certain conditions. It is worth mentioning that along with the folding models of MOP, there are also microscopic models, based on effective NN interactions, which involve the random-phase-approximation calculations, e.g., Refs. [14–16].

As an alternative to the g-matrix approach, for microscopic calculations of nuclear structure and characteristics of nuclear matter the effective density-dependent NN interactions of the Skyrme type [17] are widely used, starting from Ref. [18]. Great efforts have been devoted to the further elaboration of variants of Skyrme NN forces (see, for example, Refs. [19,20] and references therein), which could be able to simultaneously describe different properties of nuclei, including exotic nuclei, and properties of excited nuclear states, and were suitable for astrophysical problems, such as calculations of neutron stars. It is also advisable to consider the possibility of application of these effective Skyrme NN forces in calculations describing nuclear scattering processes instead of the usually employed g-matrix interactions; examples of such calculations can be found, in particular, in Refs. [15,16].

Such an approach to analyzing NA scattering, basing on the density-dependent Skyrme NN forces, was developed in Refs. [21–25], making use of the corresponding microscopic NA optical potentials found from approximate calculations of the mass operator of the one-particle Green's function by perturbation theory. In our papers [22–24], the real part of the NA MOP was used in the form of the finite-nucleus potential, calculated in the Hartree-Fock approximation with the Skyrme forces (SHF) of the standard form [18], while the imaginary part of the MOP was calculated in the nuclear-matter and local-density approximations; in Ref. [25] this approach was further employed with extended-form Skyrme forces of the type in Refs. [26,27], allowing for the both density- and momentum-dependent terms. It is essential that in

*vpilipenko@kipt.kharkov.ua

Refs. [22–25] we used the self-consistent calculations of the NA MOP and nucleon densities of the target nucleus. On this basis, we succeeded in satisfactorily describing differential cross sections and analyzing powers of the elastic neutron- and proton-nucleus scattering at medium energies as well as the NA reaction cross sections by means of finding new optimized sets of parameters of the Skyrme forces.

Comparing this MOP model based on the Skyrme forces with the above-mentioned folding-model approach, which uses the complex g-matrix interaction (see, e.g., Refs. [3,5–7,13]), it worth noting the following points. The effective NN interaction used in these folding models is built proceeding from certain realistic NN interactions by means of approximately solving the corresponding equation for the g matrix in nuclear matter, whereas the effective Skyrme interaction is parametrized, with the involved parameters being determined by optimizing the description of certain sets of experimental data. Because the employed effective Skyrme interaction is purely real, in contrast to these folding models, it is necessary to calculate the imaginary part of MOP separately, which is done by considering the second-order Goldstone diagrams. Another essential distinction of the approach under consideration consists in using the same effective NN forces both for describing the interaction between the incident nucleon and bound nucleon in the target and for calculating the needed nuclear densities, while in the folding models the employed g-matrix interaction is used for the first purpose, but the nuclear target structure is described independently, for example, calculated with other effective NN forces. Thus, the considered model attempts to implement a unified approach including both the shell model of nuclei and the MOP describing the nuclear scattering.

Since the approach [21–25] to building the NA MOP with the Skyrme forces is successful in describing the observables of neutron-nucleus (nA) and proton-nucleus (pA) scattering, it is possible to generalize it for analyzing scattering processes with composite light ions. On this route, in works of Refs. [28–30] calculations of cross sections of the deuteron, ^{3}He, and ^{4}He elastic scattering on nuclei were performed in the framework of consideration eventually resulting in the single-folding model with NA MOP from Ref. [21]. In Ref. [31] we also performed an analysis of the cross sections and different spin observables for the elastic deuteron-nucleus (dA) scattering within the SFM with the NA MOP from Ref. [25]. It is necessary to stress that there are essential distinctions between our approach [22–25,31] and that of Refs. [21,28–30]: In the latter the real part of NA MOP is calculated in the nuclear-matter and local-density approximations and does not take account of the rearrangement potential, arising in the SHF approximation with the density-dependent NN forces, and these calculations are not self-consistent, in contrast to our approach.

Because the generalization of our self-consistent model for the case of the dA MOP turned out to be sufficiently successful in describing experimental dA scattering data (see Ref. [31]), it is interesting to apply it also to analyzing the ^{4}He $+A$ scattering, which could yield useful information for developing a unified approach to the description of scattering processes and nuclear structure. For this reason, in the present article we consider the αA MOP constructed in the SFM, based on the NA MOP obtained in our self-consistent approach with Skyrme forces. We use this αA MOP to describe the elastic and inelastic αA scattering and study the applicability of various variants of Skyrme NN forces, including the optimized variants found by the authors in Refs. [23,25] from analyzing the elastic NA scattering observables and characteristics of nuclear structure.

II. THE MODEL OF αA MOP WITH THE SKYRME INTERACTION

The method of constructing the MOP for describing the αA scattering is based on the model of NA MOP developed by us earlier in Refs. [22–25], using approximate calculations of the mass operator of the one-particle Green's function with the Skyrme forces depending on the nuclear density. We will use the approximations that reduce the αA MOP calculation scheme to the single-folding approach, which was frequently used in the literature for describing scattering of composite particles, in particular ^{4}He, by nuclei.

Note that in Ref. [30] a theoretical scheme was considered in which the αA MOP was identified with the mass operator of the four-particle Green's function in the nuclear medium. Examining the corresponding Goldstone diagrams up to second order inclusive, the authors of Ref. [30] ignored the contributions containing the direct interaction between nucleons in the projectile, considering ^{4}He as a cluster. Moreover, they also neglected the contributions including the indirect interactions of the nucleons in ^{4}He, which can lead to the ^{4}He breakup. As a result of these approximations, in Ref. [30] the αA optical potential was represented in the single-folding form with the NA MOP from the model of Ref. [21] calculated on the basis of the Skyrme forces in the approximations of nuclear matter and local density, and this αA MOP was used for analyzing the experimental elastic αA scattering cross sections.

On the other hand, in a number of papers (see, for example, Ref. [7] and references therein) it was noted that, when applying the SFM for obtaining optical potentials for composite projectiles, certain corrections to the potentials can be necessary, which are mainly reduced to renormalization of the SFM potentials and are attributed to several physical effects of the composite structure of the incident nuclei. However, we have in mind the results of Ref. [6], which showed that the scattering cross sections calculated in the SFM approximation could be sufficiently close to those in the DFM calculations in certain α-particle energy regions, in particular at energies lower 120 MeV, and the αA optical potentials obtained in the both models required no renormalization to reproduce the considered experimental data. For this reason, here we also hope to do without such renormalizations of our αA MOP and will not consider them.

Taking into account the above reasoning, the MOP for describing the ^{4}He scattering on nuclei can be presented in the following single-folding form:

$$U_{\alpha A}(R) = 2\int d^3r_\alpha \left\{\rho_n^{(\alpha)}(\mathbf{r}_\alpha)U_n(|\mathbf{R}+\mathbf{r}_\alpha|,E) + \rho_p^{(\alpha)}(\mathbf{r}_\alpha)U_p(|\mathbf{R}+\mathbf{r}_\alpha|,E)\right\}. \quad (1)$$

Here $\rho_q^{(\alpha)}(\mathbf{r}_\alpha)$, where $q = n, p$, are the neutron and proton one-particle densities (normalized to unity) for the incident ^{4}He nucleus and $\mathbf{r}_\alpha$ is the nucleon coordinate in the projectile from its center of mass (c.m.); $U_q(r_q, E)$ are the nA and pA optical potentials depending on the incident nucleon energy E; and $\mathbf{R}$ is the vector from the c.m. of the target nucleus to that of the projectile. In the present study, the microscopic NA potentials U_q will be employed in the form found by us in Ref. [25] on the basis of calculations using the effective Skyrme NN interaction, which is taken, in general, in the following extended form:

$$\begin{aligned} v = {} & t_0(1 + x_0 P_\sigma)\delta(\mathbf{r}) + \tfrac{1}{2}t_1(1 + x_1 P_\sigma)[\mathbf{k}'^2\delta(\mathbf{r}) \\ & + \delta(\mathbf{r})\mathbf{k}^2] + t_2(1 + x_2 P_\sigma)\mathbf{k}'\delta(\mathbf{r})\mathbf{k} + \tfrac{1}{6}t_3(1 + x_3 P_\sigma) \\ & \times \rho^\gamma(\tilde{\mathbf{R}})\delta(\mathbf{r}) + i W_0(\boldsymbol{\sigma}_1 + \boldsymbol{\sigma}_2)[\mathbf{k}' \times \delta(\mathbf{r})\mathbf{k}] \\ & + \tfrac{1}{2}t_4(1 + x_4 P_\sigma)[\mathbf{k}'^2\rho^{\gamma_4}(\tilde{\mathbf{R}})\delta(\mathbf{r}) + \delta(\mathbf{r})\rho^{\gamma_4}(\tilde{\mathbf{R}})\mathbf{k}^2] \\ & + t_5(1 + x_5 P_\sigma)\mathbf{k}'\rho^{\gamma_5}(\tilde{\mathbf{R}})\delta(\mathbf{r})\mathbf{k}. \end{aligned} \quad (2)$$

Here $\mathbf{r}$ and $\tilde{\mathbf{R}}$ are the relative and c.m. coordinates of the two interacting nucleons; $\rho = \rho_n + \rho_p$, ρ_n, and ρ_p are the total, neutron, and proton densities of the target nucleus; $\mathbf{k} = -i\partial/\partial\mathbf{r}$ and $\mathbf{k}' = i\partial/\partial\mathbf{r}'$ are the momentum operators of the relative nucleon motion in the initial and final states; and P_σ is the operator of spin permutation. The quantities t_n, x_n ($n = 0 - 5$), γ, γ_4, γ_5, and W_0 are the phenomenological parameters of the NN interaction. In Eq. (2), the terms in the first three lines correspond to the standard form of Skyrme force and the last two lines present the momentum- and density-dependent terms with parameters t_4 and t_5.

The expressions for the potentials $U_q(r_q, E)$ are obtained from calculations of the mass operator of the one-particle Green's function by perturbation theory up to the Goldstone diagrams of second order inclusive [22,23,25], where the mean self-consistent Hartree-Fock (HF) potential is taken as the zeroth-order approximation. In the SHF theory, the variation of the HF functional with the effective nuclear-density-dependent NN forces results in the rise of the so-called rearrangement potential, which plays an important role in ensuring the nuclear force saturation and is taken into account in our approach [22–25,31], in contrast to that of Refs. [21,28–30]. Constructing the αA MOP, we do not take account of the NA spin-orbit potential, and therefore, the NA optical potentials $U_q(r, E)$ for the incident nucleons of sort q can be represented as follows:

$$U_q(r, E) = V_q(r, E) + i W_q(r, E) + \delta_{q,p}\frac{m_q^*(r)}{m_q}V_C(r), \quad (3)$$

where the real central part of the NA MOP has the form

$$\begin{aligned} V_q(r, E) = {} & \frac{m_q^*(r)}{m_q}[V^{(\mathrm{HF})}(r) + V^{(m)}(r)]_q \\ & + \left(1 - \frac{m_q^*(r)}{m_q}\right)\frac{M}{M + m_q}E. \end{aligned} \quad (4)$$

Here m_q and E are the mass and laboratory energy of the incident nucleon and M is the target-nucleus mass. The central $V^{(\mathrm{HF})}(r)$ and Coulomb $V_C(r)$ potentials are calculated according to the SHF theory for finite nuclei and $m_q^*(r)$ is the effective mass of the nucleon inside the nucleus. The term $V^{(m)}(r)$ arises in the transformation from the nonlocal HF equation to the Schrödinger equation with energy-dependent local potential [32] and is expressed through the effective mass m_q^*. The expression for the imaginary part of the NA MOP $W_q(r, E)$ is obtained from the second-order Goldstone diagrams and is calculated in the approximations of nuclear matter and local density. It includes dependence on the nucleon density ρ and on certain integrals over the momenta of intermediate nucleon states in these diagrams. These latter integrals depend on the nucleon densities ρ_n and ρ_p and on the magnitude of the incident-nucleon wave vector k being related to the nucleon energy E by the following dispersion law:

$$k^2 = \frac{2m_q^*}{\hbar^2}\left[\frac{ME}{M + m_q} - V^{(\mathrm{HF})} - V_C\right]. \quad (5)$$

The explicit expressions for all above-mentioned potentials, calculated with the Skyrme forces (2), are given in Eqs. (5)–(20) of Ref. [25] and we do not present them here. The densities $\rho_{n,p}(r)$, the kinetic-energy densities $\tau_{n,p}(r)$, and the spin densities $J_{n,p}(r)$ of nucleons [18], which are necessary for calculating these potentials, are obtained from the self-consistent calculations of the target-nucleus structure by the SHF method using the same Skyrme force (for details, see Ref. [25]).

When calculating the αA MOP with Eq. (1), we choose the nucleon energy in the used NA MOP to be $E = E_\alpha/4$, where E_α is the energy of incident α particles, as it is made in the majority of works considering αA scattering.

In our calculations, we assume, for the sake of simplicity, that the proton and neutron densities $\rho_{n,p}^{(\alpha)}(r)$ for ^{4}He are equal to each other and can be taken in the Gaussian form:

$$\rho_{n,p}^{(\alpha)}(r) = \frac{1}{(\pi b^2)^{3/2}}\exp(-r^2/b^2). \quad (6)$$

This distribution of the nucleon density in ^{4}He is a frequently used one (see, for example, Refs. [1,4,7]) and can be considered as sufficiently acceptable. We use the parameter value $b = 1.1932$ fm [1,4,7], which corresponds to the ^{4}He rms radius of 1.4614 fm and is in agreement with the experimental value of its charge radius [33].

III. CALCULATIONS OF THE ^{4}He + A SCATTERING CROSS SECTIONS

For implementing the SFM of αA MOP using the above-described model of NA MOP constructed with the effective Skyrme NN forces, we have developed an original numerical optical-model code including the SHF calculations. Using this code, we have performed an analysis of differential cross sections of the elastic scattering of α particles in the projectile-energy region up to $E_\alpha \sim 100$ MeV in a wide range of target-nucleus mass numbers. We have considered a number of up-to-date variants of the Skyrme forces of the both standard and extended form employed in studying the nuclear structure. We also examined the optimized variants SkOP (a standard Skyrme force), SkOP3, and SkOP4 (extended-form forces), obtained earlier by us from optimizing the description of the

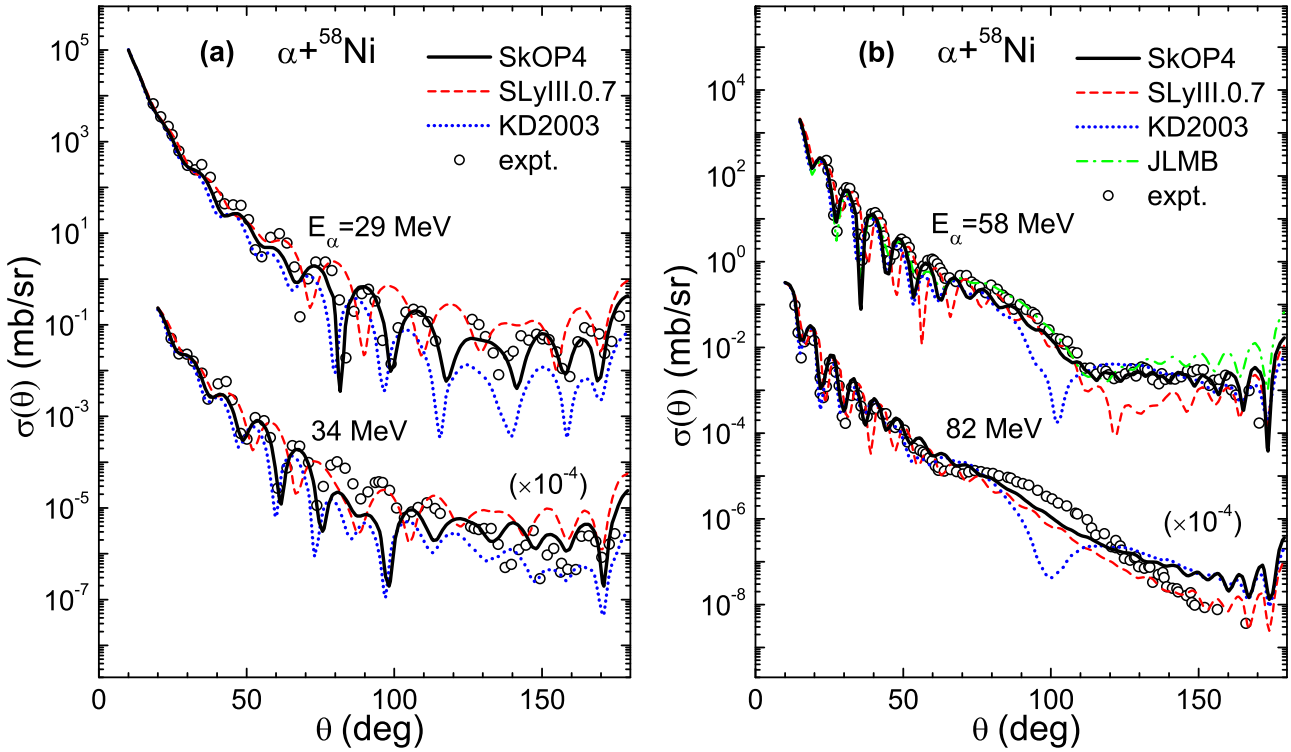

FIG. 1. Differential cross sections $\sigma(\theta) \equiv d\sigma(\theta)/d\Omega$ of the elastic α-particle scattering on ^{58}Ni nuclei at several energies calculated by the single-folding αA MOP with different NA potentials. Experimental data are from Refs. [37,38].

neutron-nucleus scattering with simultaneous control of the main characteristics of the nuclear matter and structure of finite nuclei. These optimized forces ensured a satisfactory description of the cross sections and polarizations of nA and pA scattering together with acceptably reproducing characteristics of nuclear structure, as well as a reasonable

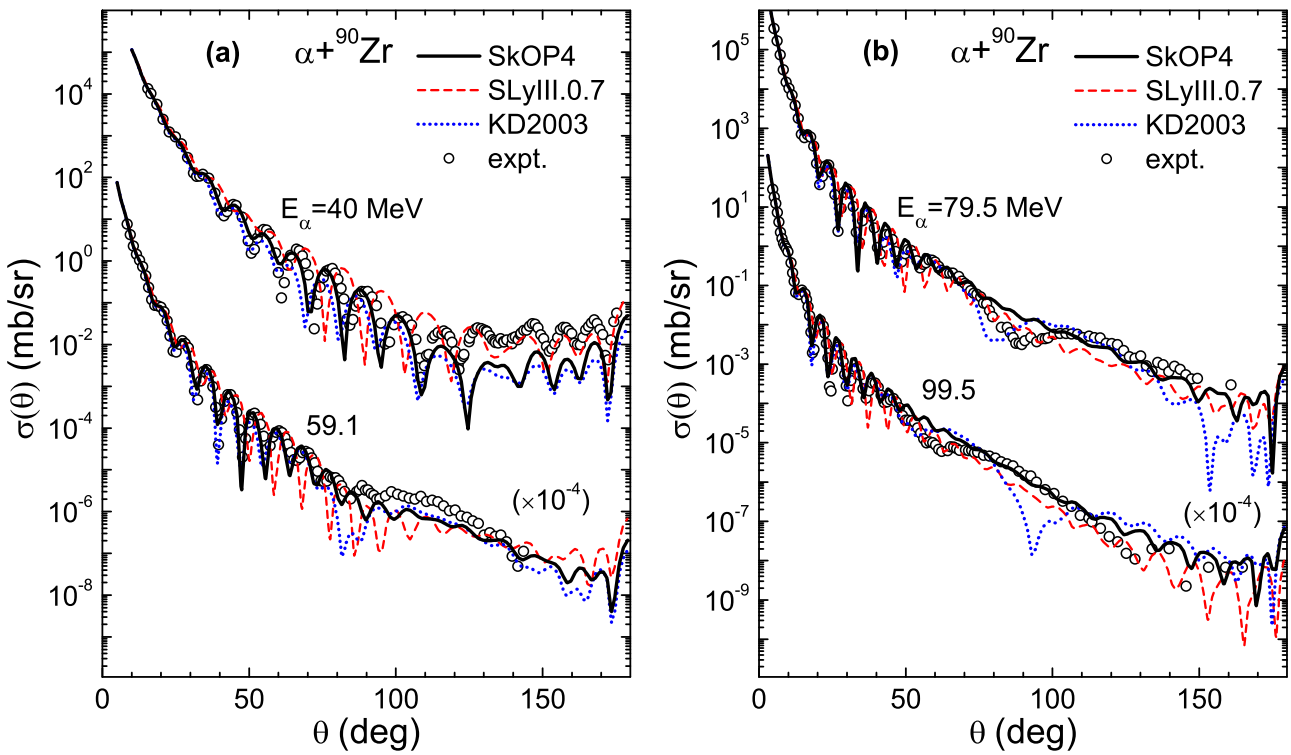

FIG. 2. The same as in Fig. 1, but on ^{90}Zr. Experimental data are from Ref. [39].

description of various observables for the dA scattering (see Refs. [25,31]).

From all considered Skyrme force variants, both those from the literature and our optimized ones, we have chosen the extended force variant SkOP4 (SkOP3 yields similar results) and the standard variant SLyIII.0.7 (results with SLyIII.0.8 are also close) [34], which give, in our opinion, the best description of experimental data. Therefore, below we present results of calculations only for these force variants in comparison with the SFM calculations basing on the global phenomenological NA optical potential [35] (denoted as KD2003). This global potential ensures a successful description of observables of the elastic NA scattering, which is, on the whole, better than the description by our NA MOP with Skyrme forces, and therefore, we consider this comparison as an additional test of applicability of our NA MOP in the αA scattering calculations. The experimental data on cross sections were mainly taken from the electronic nuclear reaction database [36].

In Figs. 1–4, we present the results of calculations by the considered model of αA MOP for the differential cross sections of the elastic α-particle scattering at different projectile energies on different target nuclei (here and below the numbers in parentheses are the offsetting factors for the cross sections). As can be seen from Figs. 1–4, in general, the calculations with our optimized extended-form force variant SkOP4 yield a reasonable description of the experimental data, being somewhat better than when using the standard SLyIII.0.7 force. Note that calculations of NA and dA scattering observables basing on the SLyIII.0.7 force give

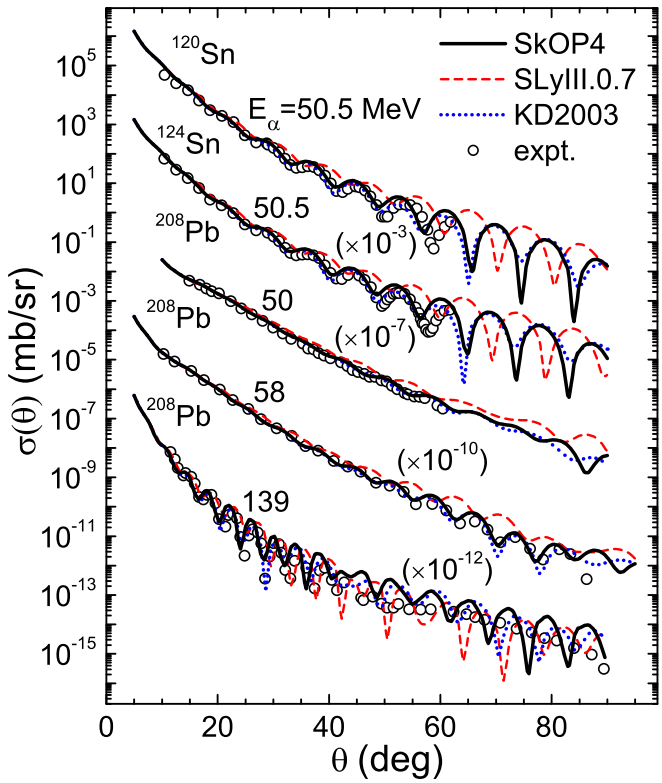

FIG. 3. The same as in Fig. 1, but for ^{120,124}Sn and ^{208}Pb target nuclei. Experimental data are from Refs. [40–43].

results close to those obtained with SLyIII.0.8, which provide a reasonable description of the NA and dA data, being not much worse than for the results obtained with our optimized force variants (see Ref. [31]). However, in the case of $\alpha + A$ scattering under consideration, the calculations on the basis of αA MOP with using extended-form SkOP4 (or SkOP3) force better agree with the experimental data than when using all standard-form forces considered by us, including our optimized variant SkOP. At the same time, the αA MOP with the extended Skyrme force variants from Ref. [27] do not give a satisfactory description of the data, so we do not present results for them here. Note that the extended forces SkOP3 and SkOP4 also yielded somewhat better results in describing the NA scattering than our optimized standard-form variants, whereas they had no advantage in the case of dA scattering (see Refs. [25,31]). It may be somewhat surprising that making use of the SFM with the approved global NA potential KD2003 gives even a worse description of the elastic αA scattering cross sections than the calculations on the basis of the SkOP4 force. In the further figures we shall show results of calculations using only this Skyrme force SkOP4.

The calculation results in Figs. 1–4 are shown for E_α values in a rather wide energy range. We may note that in Fig. 1, for the $\alpha + {}^{58}$Ni scattering at lower energies of 29 and 34 MeV, the model with Skyrme forces gives somewhat worse agreement with the data than in other considered cases. In this connection, we should remind readers that the used optimized SkOP4 force was found in Ref. [25] from fitting the differential cross section and analyzing power of elastic $n + {}^{120}$Sn scattering at the neutron energy of $E = 13.9$ MeV. In Ref. [25] the best description of experimental data on cross sections and analyzing powers of the neutron scattering on different target nuclei was obtained at the energies $E_n < 20$ MeV, and for the pA scattering this model yielded satisfactory results also at somewhat higher energy values. However, in the case of the pA scattering there arises a certain limitation of this model at small energies owing to the existence of the Coulomb barrier in the real pA potential, which is most essential for heavy target nuclei. It was pointed out in Refs. [22–25] that in the region of higher energies of incident nucleons an excessive growth of the depth of imaginary part of NA MOP (the nuclear absorption) occurs. For these reasons, this model of NA MOP is expected to be mostly applicable for constructing the αA MOP at energies of α particles below or about 100 MeV, which corresponds to the nucleon-energy region, where it works well enough for describing both the nA and pA scattering.

It is worth mentioning that in Fig. 1 the calculations by means of the αA MOP with SkOP4 force reproduce the nuclear-rainbow-like refractive damping of diffraction oscillations (see, for example, Refs. [43,46]) observed in the $\alpha + {}^{58}$Ni scattering cross section at 58 MeV in the region of sufficiently large angles. Note that in calculations with the SLyIII.0.7 force this effect is described somewhat worse. It should be remarked that the NA MOP with the SkOP4 force used here also works well enough in describing the nA and pA observables at the incident nucleon energies close to the value $E_\alpha/4$, which can be clearly seen in Figs. 6, 7, 9, and 10 of Ref. [25].

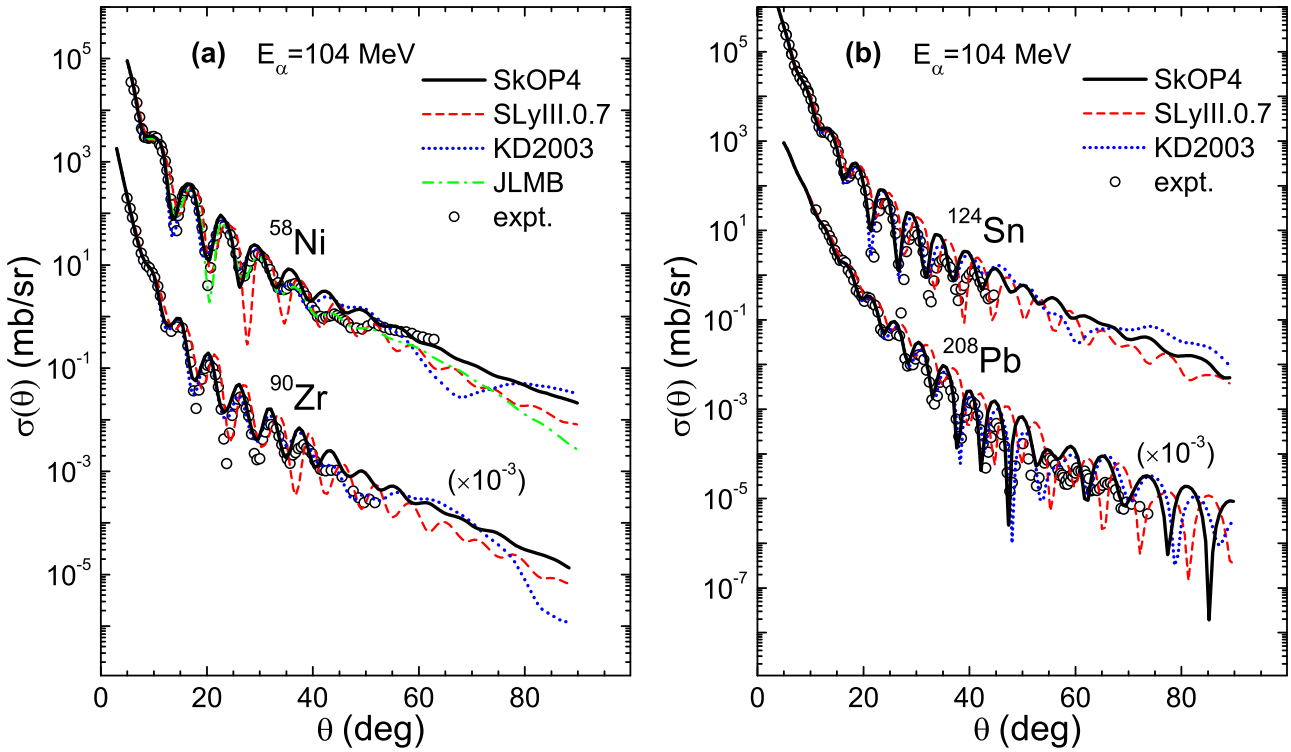

FIG. 4. The same as in Fig. 1, but for ^{58}Ni, ^{90}Zr, ^{124}Sn, and ^{208}Pb target nuclei at 104 MeV. Experimental data are from Refs. [44,45].

At the higher energy 82 MeV, the calculations with Skyrme forces also lead to a refractive damping of cross section oscillations, but they do not describe properly the rainbow hump observed in the experimental cross section in the angle region 80–100°, and this discrepancy indicates that the transparency of the target nucleus at small impact parameters is too small, i.e., nuclear absorption is too large. The damping of oscillations in this calculated cross section is characteristic of the effect of nuclear refraction in the nucleus surface region [46].

In the case of the $\alpha + ^{90}$Zr scattering at 59.1, 79.5, and 99.5 MeV (see Fig. 2) the calculated cross sections also demonstrate a similar refractive damping of diffraction oscillations. Note that the calculations with the SFM model using the global NA potential KD2003, in most cases, give a worse description of the mentioned refraction effects. We also call attention to the pronounced diffraction oscillations of the calculated $\alpha + ^{208}$Pb scattering cross section at the higher energy 139 MeV (see Fig. 3). These oscillations disagree with the experimentally observed refractive pattern at the angles $\theta > 50^\circ$ and are obviously a consequence of the excessively deep imaginary part of MOP. In Fig. 4 we also present examples of calculations at a rather large energy of 104 MeV.

It is also interesting to compare the behavior of the αA MOP variants used in calculations of the above-presented cross

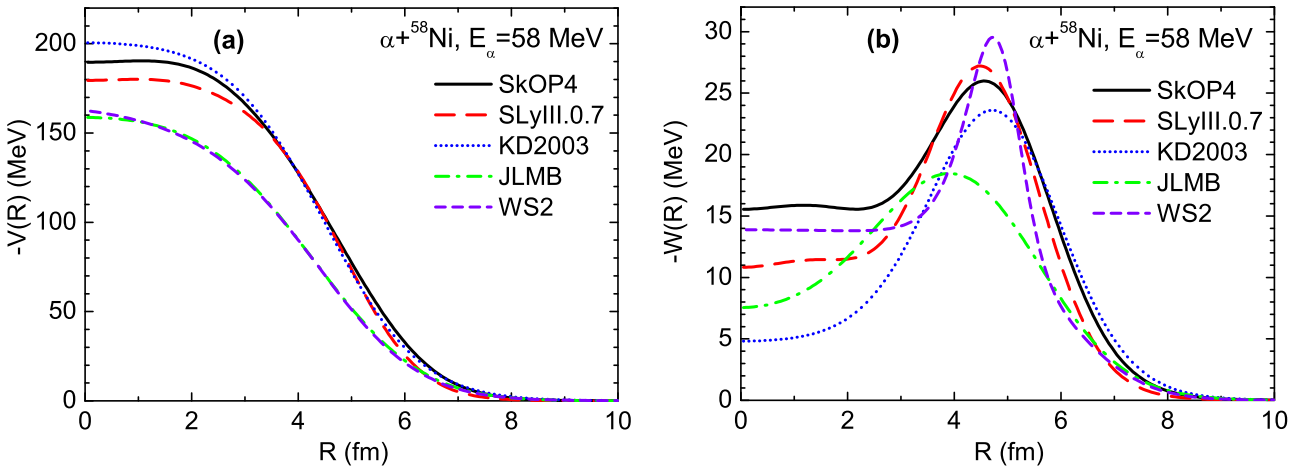

FIG. 5. Radial dependences of the (a) real $V(R)$ and (b) imaginary $W(R)$ parts of different optical potentials (for details see the text) for the $\alpha + ^{58}$Ni scattering at the projectile energy 58 MeV.

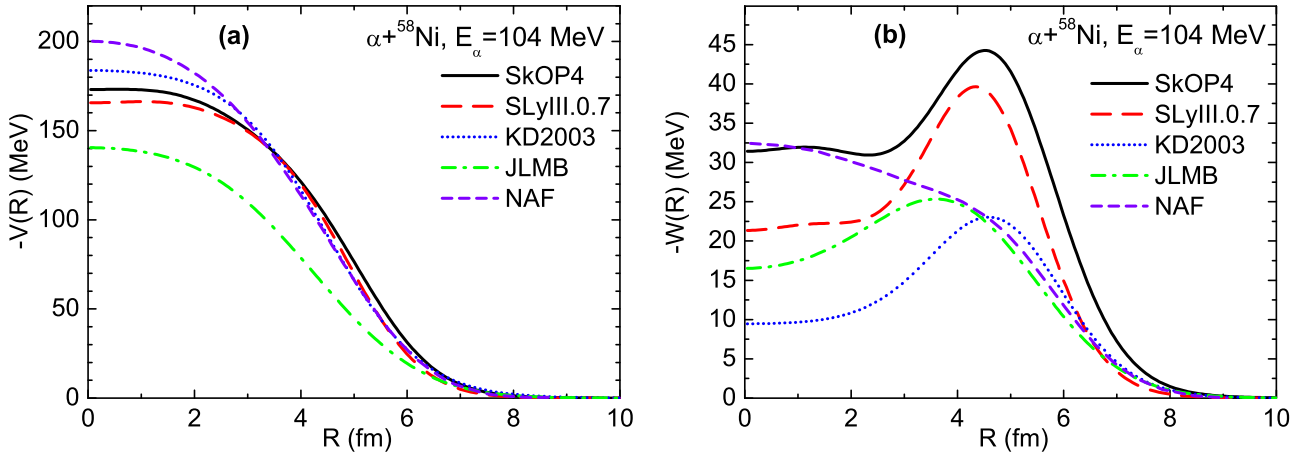

FIG. 6. The same as in Fig. 5, but at the projectile energy 104 MeV.

sections together with other examples of appropriate optical potentials from literature. For this purpose, we present such a comparison of real and imaginary parts of different optical potentials for two considered cases, namely, for $\alpha + {}^{58}$Ni scattering at 58 MeV in Fig. 5 and at 104 MeV in Fig. 6. In both these figures, we also present the single-folding potentials obtained by the model used in Ref. [7], which employs the Lane-consistent NA MOP of Ref. [47] based on the approach of Ref. [13] and implemented in the numerical code MOM [48]. We have calculated these $\alpha + {}^{58}$Ni MOP (denoted as JLMB) using the SHF calculations with our SkOP4 force for the nucleon densities needed in the code MOM, while the values of the renormalization factors N_r and N_i and range parameter t_{ri}, entering into this model, were taken from Table III of Ref. [7]: $N_r = 0.77$, $N_i = 0.87$, and $t_{ri} = 1.41$ fm at 58 MeV and $N_r = 0.73$, $N_i = 1.05$, and $t_{ri} = 1.43$ fm at 104 MeV. The $\alpha + {}^{58}$Ni scattering cross sections calculated with these JLMB potentials are shown in Figs. 1(b) and 4(a), the result at 58 MeV being rather close to the result of analogous calculation available in Ref. [7]. In Fig. 5, we also show the best-fit phenomenological potential from Ref. [37] at 58 MeV (denoted as WS2), which uses the Woods-Saxon-square form for real and volume imaginary potentials and the derivative of the Woods-Saxon-square form for the surface imaginary part. Figure 6 also shows the curves for the single-folding $\alpha + {}^{58}$Ni MOP at 104 MeV taken from Fig. 6 of Ref. [6], denoted as NAF. This MOP employs the NA folding potential based on the Melbourne g-matrix interaction of Ref. [3]. As can be seen from Figs. 5 and 6, the presented optical potentials contain essential distinctions, even when they yield comparable descriptions of the experimental data. At the energy of 58 MeV, our potentials obtained with the Skyrme forces SkOP4 and SLyIII.0.7 slightly differ in their real and surface imaginary parts, whereas there is a more significant distinction in the volume imaginary part at smaller R values. At the same time, the phenomenological WS2 potential provides a reasonable description of this cross section, including the mentioned refraction effects, by means of a considerably less deep real potential and the surface imaginary part that also essentially differs. It is interesting that the JLMB MOP, which also describes these data well, has the real part very close to that of WS2, while its imaginary part markedly differs not only from our MOP variants but also from the WS2 potential. At 104 MeV our MOP variants drastically differ from the JLMB MOP. However, their real parts are close to the real part of the NAF potential in the surface region, and the imaginary part of our MOP based on the SkOP4 force approaches the imaginary part of NAF at smaller R values. The main distinction of our MOP is too deep surface imaginary part, which is absent in the NAF potential. This large surface imaginary potential in our MOP at 104 MeV illustrates the above-stated shortcoming of the present model consisting in the excessive growth of the nuclear absorption with the energy increase.

It is also useful to check up the validity of the αA microscopic optical potential by calculating the total reaction cross sections σ_r, which are an important characteristic of the α-particle interaction with nuclei. Thus, we have performed calculations of σ_r by the proposed model for several target nuclei in a rather wide range of the incident α-particle

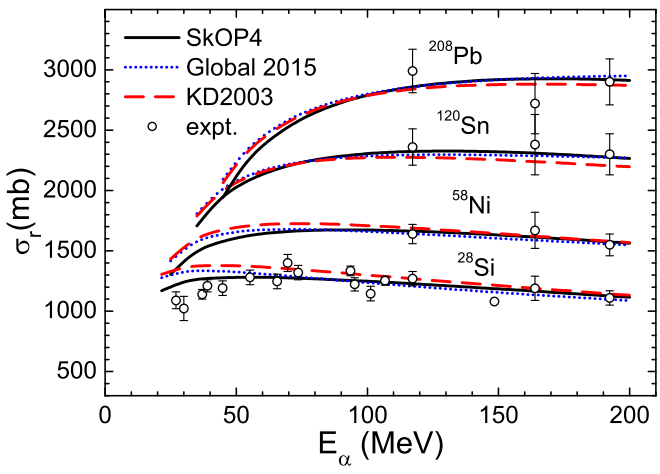

FIG. 7. Reaction cross sections σ_r for the α-particle interaction with ^{28}Si, ^{58}Ni, ^{120}Sn, and ^{208}Pb nuclei as functions of the energy E_α calculated by the αA MOP with the SkOP4 force, by the SFM using the global NA potential KD2003, as well as by means of the global αA potential. Experimental data are from Refs. [49–51].

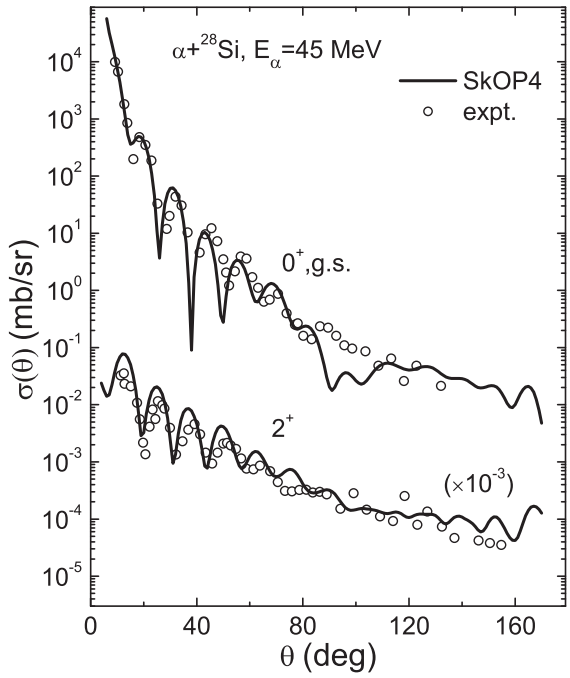

FIG. 8. Differential cross sections calculated using the αA MOP with the SkOP4 force for the elastic $\alpha + {}^{28}$Si scattering at 45 MeV as well as for the inelastic scattering with exciting the first 2^+ state of ^{28}Si nucleus. Experimental data are from Ref. [53].

energies. By way of example, in Fig. 7 we present the energy dependences of the reaction cross sections $\sigma_r(E_\alpha)$ for α-particle interaction with ^{28}Si, ^{58}Ni, ^{120}Sn, and ^{208}Pb nuclei calculated by using the αA MOP based on our optimized Skyrme force SkOP4 in comparison with σ_r obtained by the SFM using the global NA potential KD2003 and with the ones calculated with the global optical αA potential proposed in Ref. [52] (denoted as Global 2015). It is seen from Fig. 7 that the calculations using the αA MOP with the SkOP4 force describe the considered reaction cross sections quite satisfactorily up to the energy values lying essentially higher than the expected upper limit of applicability of this model and do not yield to calculations by the SFM and phenomenological optical model based on the global NA and αA potentials, respectively.

The above-described model for the αA MOP based on the Skyrme forces can be directly generalized for describing the cross sections of the inelastic $\alpha + A$ scattering with exciting low-lying collective states in the target even-even nuclei. This can be easily done by using the well-known macroscopic collective model and considering these excited states as one-phonon vibrations of the nuclear surface. Such calculations can serve as an additional useful test of applicability of the proposed approach to constructing the αA MOP. We have performed the corresponding calculations for the inelastic $\alpha + A$ scattering in the distorted-wave Born approximation (DWBA), and for this purpose we have employed the known numerical code FRESCO 2.9 [60], taking account of the Coulomb-excitation contribution, which, however, is rather insignificant. In Figs. 8–12, we present examples of such calculation results,

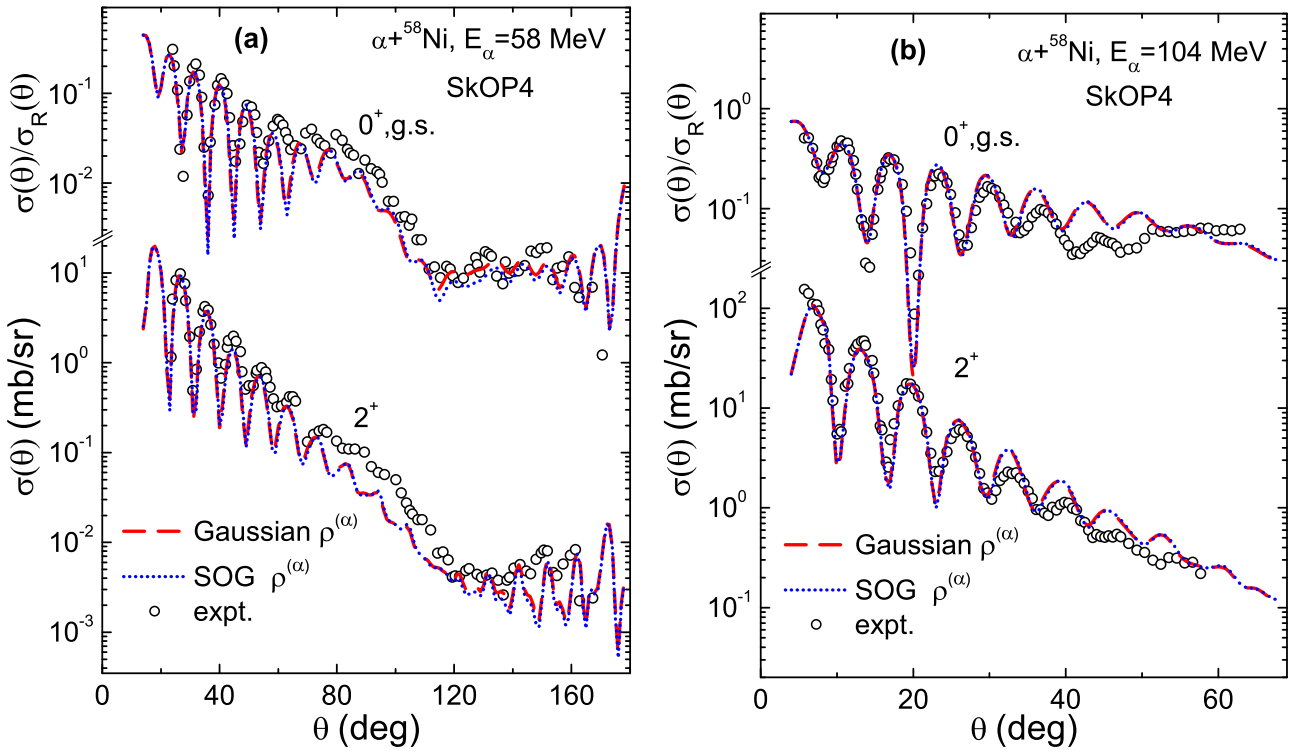

FIG. 9. The same as in Fig. 8 (the elastic cross section is normalized to the Rutherford one), but for ^{58}Ni target nuclei at (a) 58 and (b) 104 MeV, with dashed curves calculated with the Gaussian α-particle density (6) and the dotted ones with the model-free density SOG from Ref. [33]. Experimental data are from Refs. [37,44].

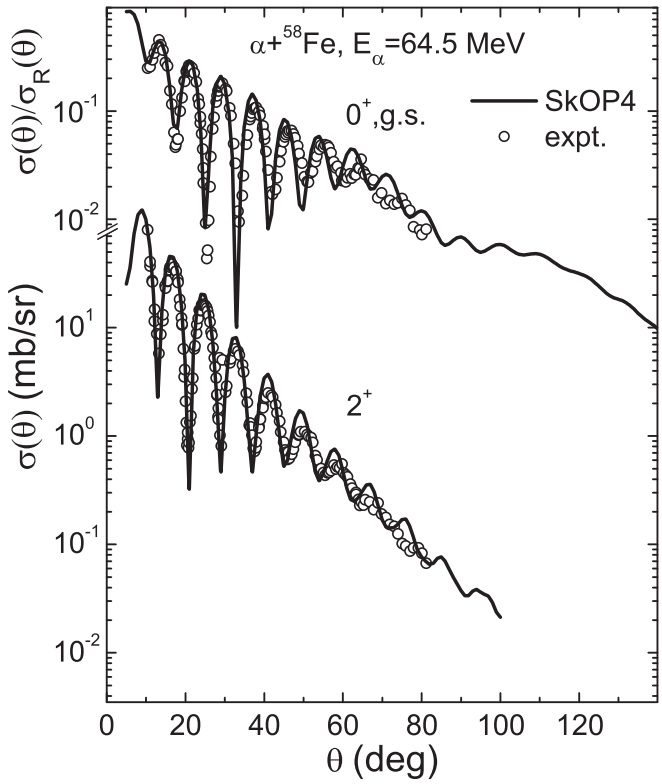

FIG. 10. The same as in Fig. 8 (the elastic cross section is normalized to the Rutherford one), but for ^{58}Fe target nuclei at 64.5 MeV. Experimental data are from Ref. [54].

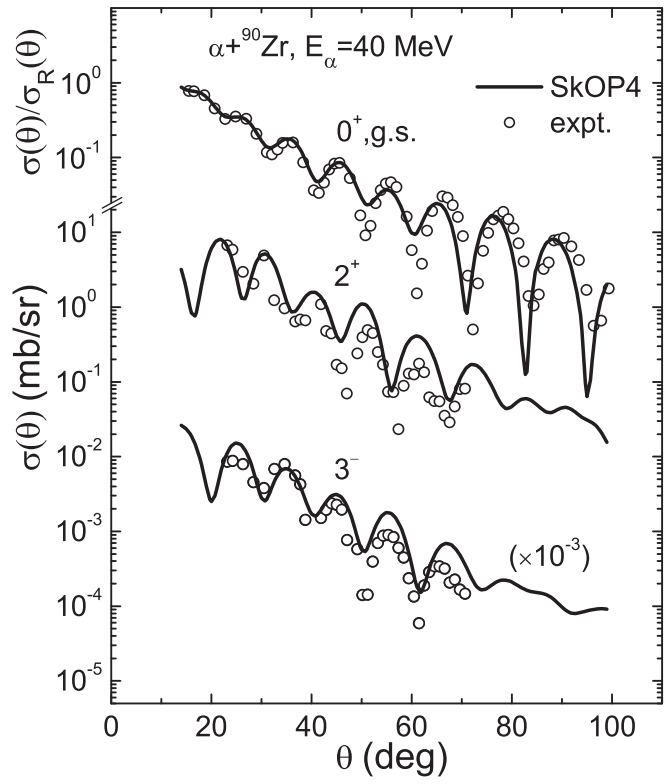

FIG. 11. Differential cross sections calculated with the SkOP4 force at 40 MeV for the elastic $\alpha + {}^{90}$Zr scattering as well as for the inelastic scattering with exciting the first 2^+ and 3^- states of ^{90}Zr nucleus. Experimental data are from Ref. [55].

obtained using the αA MOP with the SkOP4 force, for the inelastic scattering on ^{28}Si, ^{58}Fe, ^{58}Ni, ^{90}Zr, and ^{208}Pb nuclei along with the results for the corresponding elastic scattering cross sections for these target nuclei at the same projectile energies. The deformation lengths, used in the calculations of the inelastic scattering cross sections and determining their absolute normalization, were taken the same for the real and imaginary parts of the transition potential and have been determined from the known values of $B(EL)$ [57,58] of the corresponding electromagnetic transitions in the same manner as in Ref. [11], using experimental rms charge radii [33].

As seen from Fig. 8, the calculated cross sections of both elastic $\alpha + {}^{28}$Si scattering and inelastic scattering with exciting the first 2^+ state of ^{28}Si ($E_2^* = 1.78$ MeV) at $E_\alpha = 45$ MeV reasonably agree with the experimental data. The deformation length for calculating the inelastic cross section was $\delta_2 = 1.34$ fm.

In the cases of the $\alpha + {}^{58}$Ni scattering at the projectile energies of 58 and 104 MeV, shown in Fig. 9, the inelastic scattering cross sections with exciting the first level 2^+ of ^{58}Ni nucleus ($E_2^* = 1.454$ MeV) were calculated with the deformation length value $\delta_2 = 0.81$ fm. If we use the somewhat higher value $\delta_2 = 0.992$ fm from Ref. [37] in the case of $E_\alpha = 58$ MeV, this provides better normalization of this inelastic scattering cross section. It should be noted that at the energy $E_\alpha = 58$ MeV the calculated inelastic scattering cross section reasonably reproduces the refractive effects observed at sufficiently large scattering angles, as in the calculations for corresponding elastic scattering. For the sake of comparison, in Fig. 9 we also present the results of additional calculations performed with the densities $\rho_{n,p}^{(\alpha)}(r)$, determined from the model-free charge distribution of ^{4}He in the form of the sum of Gaussian functions (SOG) [33] by eliminating the effect of finite size of the proton charge distribution [59] in the standard way. We assumed that the neutron and proton densities coincide, as was in the case of the density (6). As can be seen from the figure, the results of all presented calculations with two variants of $\rho_{n,p}^{(\alpha)}(r)$ practically coincide for both elastic and inelastic scattering cross sections.

In Fig. 10, the calculated cross sections for the elastic $\alpha + {}^{58}$Fe scattering at 64.5 MeV and for the corresponding inelastic scattering with exciting the first level 2^+ of ^{58}Fe nucleus ($E_2^* = 0.81$ MeV) are in good agreement with the experimental data and also reasonably reproduce the above-mentioned refractive damping of diffraction oscillations. Here, the deformation-length value was $\delta_2 = 1.146$ fm.

In Fig. 11, which shows the results of calculations for the $\alpha + {}^{90}$Zr scattering at $E_\alpha = 40$ MeV, the inelastic scattering is considered for the cases of exciting both the first 2^+ level with $E_2^* = 2.186$ MeV and the first 3^- level with $E_3^* = 2.748$ MeV in the target nucleus. The corresponding deformation lengths have the values $\delta_2 = 0.469$ fm and $\delta_3 = 1.134$ fm. Finally, Fig. 12 considers scattering on ^{208}Pb nuclei, where the inelastic scattering is accompanied by exciting the first 3^- level with $E_3^* = 2.615$ MeV; the used deformation length

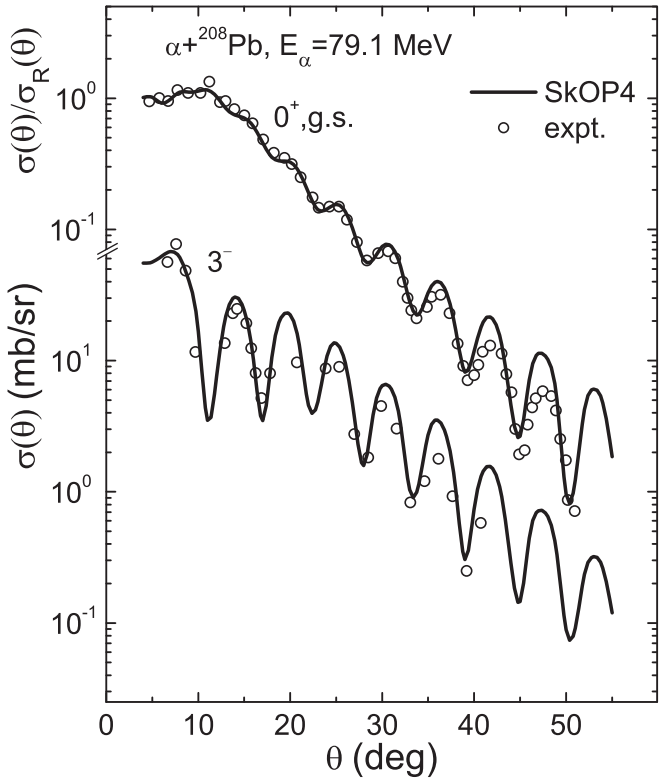

FIG. 12. Differential cross sections calculated with the SkOP4 force at 79.1 MeV for the elastic $\alpha + {}^{208}$Pb scattering as well as for the inelastic scattering with exciting the first 3^- state of ^{208}Pb nucleus. Experimental data are from Ref. [56].

was $\delta_3 = 0.793$ fm. A sufficiently good agreement with the experimental data is observed for all calculated cross sections in Figs. 11 and 12.

It should be noted that a more accurate approach to describing the inelastic scattering processes, as compared with DWBA, is the coupled-channel method (CC), which takes account of multistep effects connected with coupling between the ground and excited states, which can contribute to the elastic and inelastic cross sections and be significant at low incident energies. However, we should remember that parameters of the Skyrme forces are determined from experimental data without explicit consideration of intermediate excitations of nuclei. Their effects are partially taken into account implicitly through the found values of the Skyrme interaction parameters. In particular, as has been mentioned above, the optimization of parameters of our Skyrme force SkOP4 was performed on the basis of the self-consistent calculations of the elastic nA scattering observables and nuclear structure characteristics in the approach without explicitly considering the coupling with inelastic channels. Thus, the usage of the SkOP4 force in the CC framework, especially for obtaining the corresponding corrections to the elastic αA scattering cross sections, would not be quite consistent. For calculations by the CC, it would be necessary to use the self-consistent description of the nuclear structure and the elastic and inelastic NA scattering processes and to optimize the Skyrme force parameters with explicit consideration of the coupling between channels. For this reason, here we restrict ourselves to the DWBA description of the inelastic $\alpha + A$ scattering.

IV. CONCLUSION

We have considered a model of the microscopic optical potential, used to describe the α-particle interaction with nuclei, based on a generalization of the approach in which the microscopic optical NA potential is found from approximate calculations of the mass operator of the one-particle Green's function, employing effective NN Skyrme forces. This is made in the framework of the model of folding the single-nucleon density of ^{4}He with the NA MOP, which was earlier obtained by the authors using both the standard Skyrme forces and those of the extended form with allowance for the momentum- and density-dependent terms. This αA MOP is employed for analyzing cross sections of the α-particle scattering on even-even nuclei at medium energies in the self-consistent calculations on the basis of up-to-date Skyrme force variants, which provide simultaneously a satisfactory description of the nuclear structure in calculations by the Hartree-Fock method.

Using this approach, we have carried out calculations of the differential cross sections of the elastic scattering of α particles at the energies up to $E_\alpha \sim 100$ MeV in a wide range of mass numbers of target nuclei (from ^{28}Si up to ^{208}Pb) with using both the well-approved standard and extended Skyrme forces from the literature, as well as the NN force variants optimized earlier by us from simultaneously analyzing the elastic NA scattering observables and nuclear structure. The study has been complemented by analyzing a number of differential cross sections of the inelastic $\alpha + A$ scattering with exciting low-lying collective states in the target even-even nuclei in the same energy region. This was performed on the basis of the macroscopic collective vibrational model in the DWBA (employing the known numerical code FRESCO 2.9) with using the same αA MOP. The calculations show that the proposed model of αA MOP can provide a reasonable description of experimental data for the differential cross sections of both elastic and inelastic $\alpha + A$ scattering by different target nuclei in the considered energy region. The best agreement is obtained when using the optimized Skyrme-force variants of the extended form that were recently proposed by the authors. In some of the considered cases, the model even succeeds in reasonably reproducing the refractive structures experimentally observed in the cross sections at large scattering angles. However, it should be noted that at sufficiently high values of the projectile energy, a sufficiently accurate description of the observed refractive structures, especially of the nuclear-rainbow type, requires further improvement of the considered model of αA MOP. Presumably, this refinement could be mainly connected with eliminating certain problems caused by a too rapid increase of the depth of the imaginary part of the NA MOP with the incident energy growth. If such an improvement is a success, further refinement of the MOP model could be tried, for example, by employing corrections obtained from the dispersion relation between the real and imaginary parts of the MOP.

The applicability of the considered model of the αA MOP has also been checked in calculations of the energy

dependences of the total $\alpha + A$ reaction cross sections for several target nuclei in a wide range of mass numbers. It has been shown that these calculations based on our optimized extended Skyrme forces describe the considered reaction cross sections quite satisfactorily in a rather wide range of the incident α-particle energies (up to 200 MeV).

[1] G. R. Satchler and W. G. Love, Phys. Rep. **55**, 183 (1979).
[2] M. E. Brandan and G. R. Satchler, Phys. Rep. **285**, 143 (1997).
[3] K. Amos, P. J. Dortmans, H. V. von Geramb, S. Karataglidis, and J. Raynal, in *Advances in Nuclear Physics*, Vol. 25, edited by J. W. Negele and E. Vogt (Plenum, New York, 2000), p. 275.
[4] D. T. Khoa, Phys. Rev. C **63**, 034007 (2001).
[5] T. Furumoto and Y. Sakuragi, Phys. Rev. C **74**, 034606 (2006).
[6] K. Egashira, K. Minomo, M. Toyokawa, T. Matsumoto, and M. Yahiro, Phys. Rev. C **89**, 064611 (2014).
[7] D. Y. Pang, Y. L. Ye, and F. R. Xu, Phys. Rev. C **83**, 064619 (2011).
[8] G. Bertsch, J. Borysowicz, H. McManus, and W. G. Love, Nucl. Phys. A **284**, 399 (1977).
[9] N. Anantaraman, H. Toki, and G. F. Bertsch, Nucl. Phys. A **398**, 269 (1983).
[10] A. M. Kobos, B. A. Brown, P. E. Hodgson, G. R. Satchler, and A. Budzanowski, Nucl. Phys. A **384**, 65 (1982).
[11] A. M. Kobos, B. A. Brown, R. Lindsay, and G. R. Satchler, Nucl. Phys. A **425**, 205 (1984).
[12] D. T. Khoa, G. R. Satchler, and W. von Oertzen, Phys. Rev. C **56**, 954 (1997).
[13] J.-P. Jeukenne, A. Lejeune, and C. Mahaux, Phys. Rev. C **16**, 80 (1977).
[14] G. P. A. Nobre, F. S. Dietrich, J. E. Escher, I. J. Thompson, M. Dupuis, J. Terasaki, and J. Engel, Phys. Rev. C **84**, 064609 (2011).
[15] T. V. Nhan Hao, B. M. Loc, and N. H. Phuc, Phys. Rev. C **92**, 014605 (2015).
[16] K. Mizuyama and K. Ogata, Phys. Rev. C **86**, 041603(R) (2012).
[17] T. H. R. Skyrme, Nucl. Phys. **9**, 615 (1959).
[18] D. Vautherin and D. M. Brink, Phys. Rev. C **5**, 626 (1972).
[19] J. Stone and P.-G. Reinhard, Prog. Part. Nucl. Phys. **58**, 587 (2007).
[20] M. Dutra, O. Lourenço, J. S. Sá Martins, A. Delfino, J. R. Stone, and P. D. Stevenson, Phys. Rev. C **85**, 035201 (2012).
[21] Q.-B. Shen, Y.-L. Han, and H.-R. Guo, Phys. Rev. C **80**, 024604 (2009).
[22] V. I. Kuprikov, V. V. Pilipenko, A. P. Soznik, V. N. Tarasov, and N. A. Shlyakhov, Phys. At. Nucl. **72**, 975 (2009).
[23] V. V. Pilipenko, V. I. Kuprikov, and A. P. Soznik, Phys. Rev. C **81**, 044614 (2010).
[24] V. V. Pilipenko, V. I. Kuprikov, and A. P. Soznik, Nucl. Phys. At. Energy **11**, 367 (2010).
[25] V. V. Pilipenko and V. I. Kuprikov, Phys. Rev. C **86**, 064613 (2012).
[26] S. Krewald, V. Klemt, J. Speth, and A. Faessler, Nucl. Phys. A **281**, 166 (1977).
[27] S. Goriely, N. Chamel, and J. M. Pearson, Phys. Rev. C **82**, 035804 (2010); **88**, 024308 (2013).
[28] H. Guo, Y. Xu, Y. Han, and Q. Shen, Phys. Rev. C **81**, 044617 (2010).
[29] H. Guo, Y. Zhang, Y. Han, and Q. Shen, Phys. Rev. C **79**, 064601 (2009).
[30] H. Guo, Y. Xu, H. Liang, Y. Han, and Q. Shen, Phys. Rev. C **83**, 064618 (2011).
[31] V. V. Pilipenko and V. I. Kuprikov, Phys. Rev. C **92**, 014616 (2015).
[32] C. B. Dover and N. Van Giai, Nucl. Phys. A **190**, 373 (1972).
[33] H. D. Vries, C. W. D. Jager, and C. D. Vries, At. Data Nucl. Data Tables **36**, 495 (1987).
[34] K. Washiyama, K. Bennaceur, B. Avez, M. Bender, P.-H. Heenen, and V. Hellemans, Phys. Rev. C **86**, 054309 (2012).
[35] A. J. Koning and J. P. Delaroche, Nucl. Phys. A **713**, 231 (2003).
[36] Experimental Nuclear Reaction Data (EXFOR), http://www-nds.iaea.org/exfor/exfor.htm
[37] A. Budzanowski, H. Dabrowski, L. Freindl, K. Grotowski, S. Micek, R. Planeta, A. Strzalkowski, M. Bosman, P. Leleux, P. Macq, J. P. Meulders, and C. Pirart, Phys. Rev. C **17**, 951 (1978).
[38] H. H. Chang, B. W. Ridley, T. H. Braid, T. W. Conlon, E. F. Gibson, and N. S. P. King, Nucl. Phys. A **270**, 413 (1976).
[39] L. W. Put and A. M. J. Paans, Nucl. Phys. A **291**, 93 (1977).
[40] K. A. Kuterbekov, I. N. Kuchtina, B. M. Sadykov, and E. I. Ismatov, Ukr. J. Phys. **49**, 841 (2004).
[41] P. David, J. Debrus, H. Essen, F. Luebke, H. Mommsen, R. Schoenmackers, W. Soyez, H. V. von Geramb, and E. F. Hefter, Z. Phys. **278**, 281 (1976).
[42] R. Tickle and W. S. Gray, Nucl. Phys. A **291**, 187 (1975).
[43] D. A. Goldberg, S. M. Smith, H. G. Pugh, P. G. Roos, and N. S. Wall, Phys. Rev. C **7**, 1938 (1973).
[44] H. Rebel, R. Löhken, G. W. Schweimer, G. Schatz, and G. Hauser, Z. Phys. **256**, 258 (1972).
[45] G. Hauser, R. Löhken, H. Rebel, G. Schatz, G. W. Schweimer, and J. Specht, Nucl. Phys. A **128**, 81 (1969).
[46] M. S. Hussein and K. V. McVoy, Prog. Part. Nucl. Phys. **12**, 103 (1984).
[47] E. Bauge, J. P. Delaroche, and M. Girod, Phys. Rev. C **63**, 024607 (2001).
[48] R. Capote *et al.*, Nucl. Data Sheets **110**, 3107 (2009).
[49] R. E. Warner, R. A. Patty, P. M. Voyles, A. Nadasen, F. D. Becchetti, J. A. Brown, H. Esbensen, A. Galonsky, J. J. Kolata, J. Kruse, M. Y. Lee, R. M. Ronningen, P. Schwandt, J. von Schwarzenberg, B. M. Sherrill, K. Subotic, J. Wang, and P. Zecher, Phys. Rev. C **54**, 1700 (1996).
[50] V. Yu. Ugryumov *et al.*, Nucl. Phys. A **734**, E53 (2004); Phys. At. Nucl. **68**, 16 (2005).
[51] A. Ingemarsson, J. Nyberg, P. U. Renberg, O. Sundberg, R. F. Carlson, A. J. Cox, A. Auce, R. Johansson, G. Tibell, D. T. Khoa, and R. E. Warner, Nucl. Phys. A **676**, 3 (2000).
[52] X.-W. Su and Y.-L. Han, Int. J. Mod. Phys. E **24**, 1550092 (2015).
[53] S. Roy, T. Dey, A. Goswami, S. N. Chintalapudi, and S. R. Banerjee, Phys. Rev. C **45**, 2904 (1992).
[54] P. Darriulat, G. Igo, H. G. Pugh, J. M. Meriwether, and S. Yamabe, Phys. Rev. **134**, B42 (1964).

[55] A. D. Duysebaev, K. A. Kuterbekov, I. N. Kuchtina, B. M. Sadykov, L. I. Slusarenko, V. V. Tokarevsky, and S. A. Fayans, Phys. At. Nucl. **66**, 599 (2003).
[56] L. L. Rutledge, Jr. and J. C. Hiebert, Phys. Rev. C **13**, 1072 (1976).
[57] S. Raman, C. H. Malarkey, W. T. Milner, C. W. Nestor Jr., and P. H. Stelson, At. Data Nucl. Data Tables **36**, 1 (1987).
[58] R. H. Spear, At. Data Nucl. Data Tables **42**, 55 (1989).
[59] H. Chandra and G. Sauer, Phys. Rev. C **13**, 245 (1976).
[60] I. J. Thompson, Comput. Phys. Rep. **7**, 167 (1988).